2 PF Ring

2-1 Operation Summary

The timetable of the PF ring and PF-AR operations in FY2010 is shown in Fig. 1. The operations of both rings were conducted as per the schedule most of the time.

The operation statistics of the PF ring are summarized in Table 1. The statistics for each fiscal year since the commencement of the operation are shown in Fig. 2. In FY2010, the total operation time and actual user time were more than 5000 h and 4000 h, respectively. The failure rate is shown in Fig. 3. In the PF ring, top-up operation becomes the normal operation mode. The beam current was usually maintained at 450.0 ± 0.1 mA, which corresponds to a current accuracy of $\pm 1 \times 10^{-4}$ at an injection repetition frequency of 1.0 Hz. Four kicker magnets were initially employed for beam injection; however, we switched to a new injection scheme that uses a single pulsed sextupole magnet to reduce the intensity fluctuation of the photon beam in January of 2011. The new scheme is quite effective for the top-up operation.

Another polarized undulator was installed in the long, straight south section and tandem undulators with five bump magnets for producing a fast-switching polarization light were completed. Machine adjustment at a switching frequency of 10 Hz was started. The orbit correction using the feed-forward method was carried out to reduce the fluctuation due to switching. We will employ the fast switching mode until October 2011.

Because one high-voltage RF power supply was found to be broken in February 2010, before the summer shutdown, the user operation was carried out using three RF cavities at a beam current of 430 mA. Fortunately, we fabricated a new power supply in the previous fiscal year. Therefore, we installed the new RF power supply during the shutdown. Thereafter, operation resumed with four cavities, at a beam current of 450 mA, which has been conducted stably and without any issues. However, a problem with the helium re-liquefier in the superconducting vertical wiggler arose in January of 2011. The wiggler beamline was closed until the measure.

Table 1 Operation statistics for the PF ring in FY2010.

	Total
Ring operation time (hr)	5032.0
Actual user time (hr)	4050.8
Machine adjustment time (hr)	958.7
Failure time (hr)	22.5

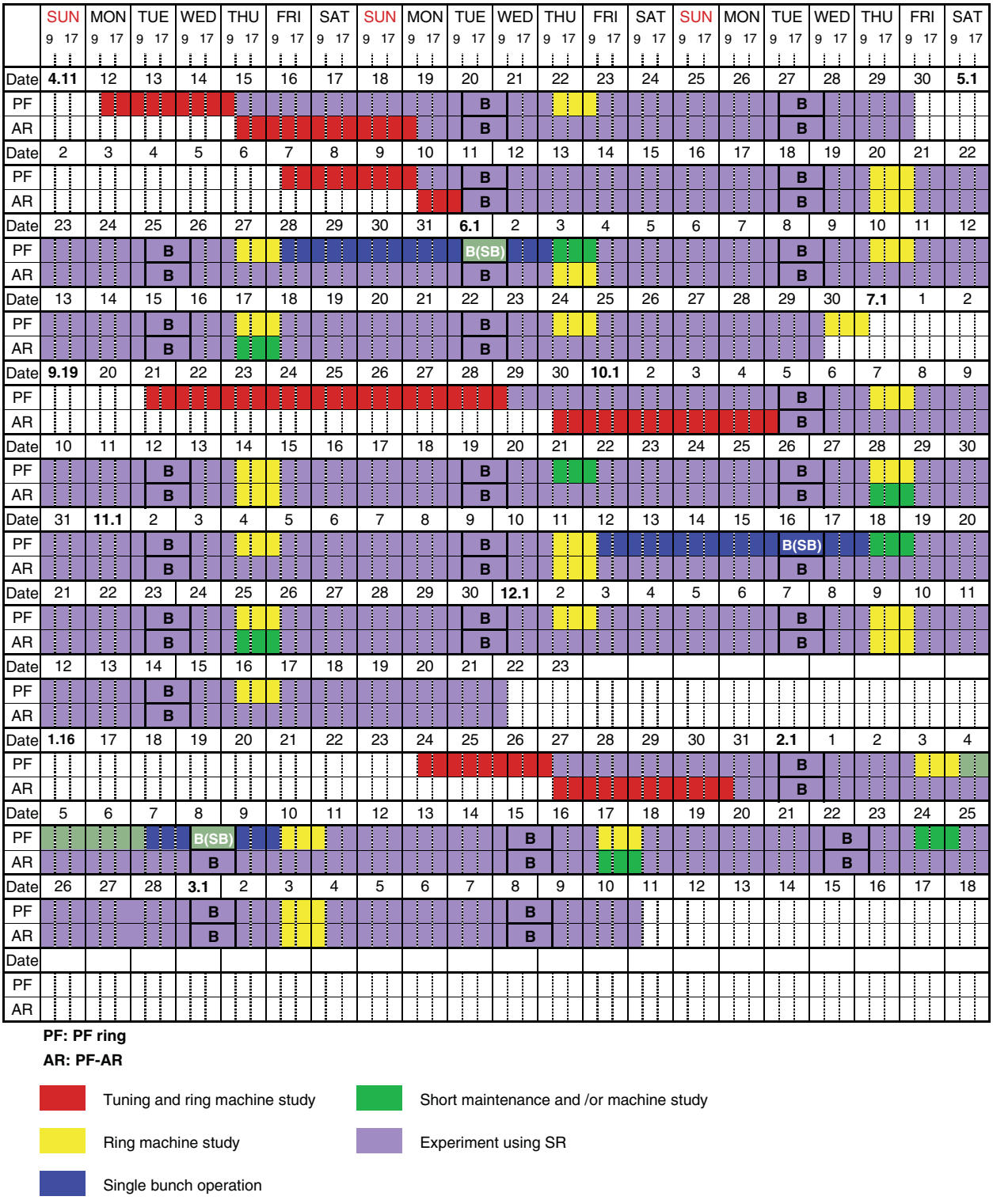

Figure 1
Timetable of PF ring and PF-AR operation in FY2010.

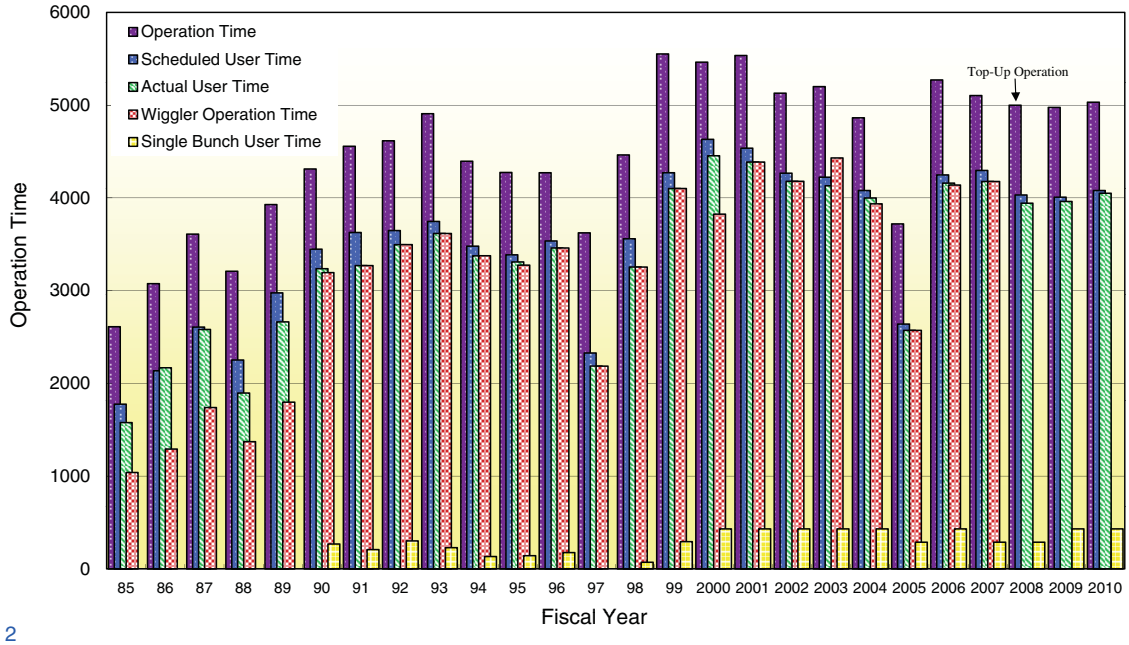

Figure 2
Total operation time, scheduled user time, actual user time, and single-bunch user time for the PF ring in each fiscal year since the commencement of operation.

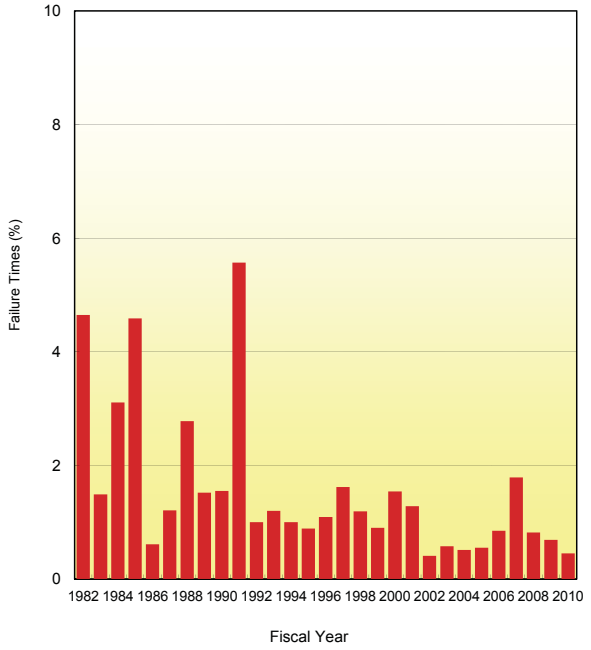

Figure 3
Failure rate for the PF ring (the ratio of the failure time to the total operation time).

2-2 Beam Profile Measurement during Pulsed Sextupole Injection

At the PF ring, a new injection scheme using a pulsed sextupole magnet (PSM) has been developed to reduce disturbance to the stored beam during top-up injection [1]. In a feasibility experiment conducted with a pulsed quadrupole magnet (PQM) at the PF-AR, it was demonstrated that dipole oscillation of the stored beam could be greatly reduced compared with the conventional kicker injection. On the other hand, beam profile modulation of the stored beam, like quadrupole mode oscillation, was clearly observed by optical measurement [2]. This profile modulation is attributed to a linear field gradient along the horizontal axis of the PQM. Using a sextupole magnet whose field gradient has a parabolic dependence instead of a quadrupole magnet is expected to reduce the profile modulation because of its smaller field around the magnetic center. In order to confirm this expectation, we measured the turn-by-turn profiles of the stored beam following an injection kick by using a fast-gated camera.

The turn-by-turn stored beam profiles were measured by observing the SR emitted from a bending magnet, BM27. BM27 is located within the injection bump orbit of the PF ring. The optical layout of the profile measurement is shown in Fig. 4. The visible light components of the SR are extracted from a vacuum chamber by a water-cooled mirror made of beryllium (Be) and fed to the optical hutch where the fast-gated camera (Hamamatsu, C4078-01 + C9164-01) is installed. The distance from the light source point in BM27 to the entrance of the focusing system is approximately 8 m. The conversion factor from pixels on CCD to meters at the source point has been calibrated by using the displacement of the source point associated with an error of the acceleration frequency of the ring. The profile measurement was performed with a single bunch of 10 mA stored in the ring. The injection kicker or the PSM installed about 30 m downstream from BM27 was fired using a tentative trigger signal without injection beams. This injection trigger was also distributed to the fast-gated camera via a digital delay module which uses the revolution frequency of the beam (1.6 MHz) as a clock. The delay module enables us to acquire the beam pro-

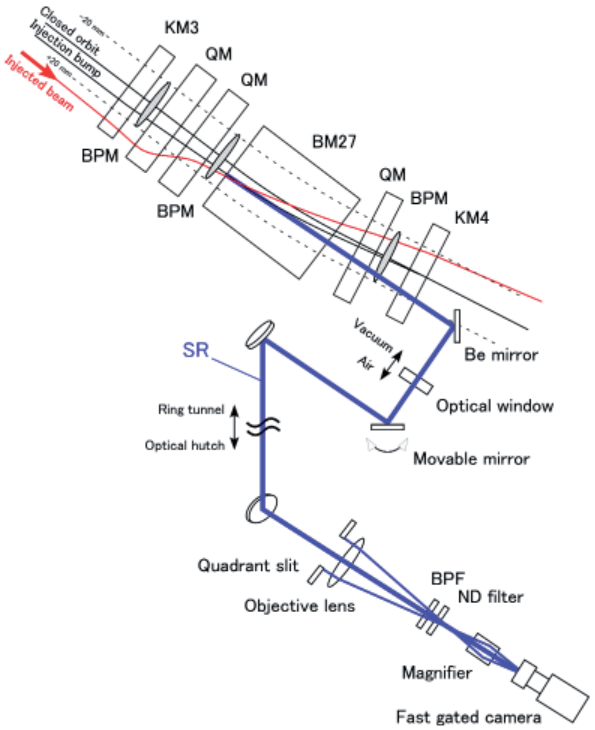

Figure 4
Optical layout of the turn-by-turn profile measurement. The blue bold line corresponds to the SR orbit. The SR source BM27 is located within the injection bump orbit produced by the four kicker magnets KM1-KM4.

file at any turn number following the injection kick. The gate width of the fast-gated camera was set to 50 ns.

The turn-by-turn stored beam profiles measured in each injection scheme are displayed in Fig. 5. Each injection magnet was fired at the first turn (turn number = 1). The upper picture corresponds to the result of the kicker injection. Large horizontal displacements observed at the first and second turns are due to the injection bump orbit [3]. Before the first turn, stable beam profiles are observed at the same position, while after the first turn, the profiles are oscillating in the horizontal plane due to the leakage of the injection bump. The middle picture shows the beam profiles in the PSM injection; almost no fluctuation in the beam position is observed after the first turn. The beam positions in the kicker and PSM injections are plotted against the turn number in Fig. 6. The origin of the vertical axis was set to the average beam position before the first turn. The amplitude of the stored beam oscillation observed in the PSM injection has been suppressed to approximately ±400 μm which is less than half of that in the kicker injection. The residual oscillation is expected to be minimized by tuning so that the stored beam precisely passes through the field center of the PSM. The stored beam oscillation excited by the leakage of the injection bump should appear almost only in the horizontal plane. However, the same level of oscillation as the horizontal plane was observed in the vertical plane. We suspect some rotation errors in the alignment of the kicker magnets and the skew quadrupole fields produced by the recently-installed undulator [4] as possible candidate sources of the strong coupling of the horizontal and vertical motions. Further studies are required to identify the source of coupling.

For reference, the result of the PQM injection obtained at the PF-AR is shown in the lower area of Fig. 5. Although there is no dipole oscillation of the stored beam as well as the PSM injection, the modulation of the beam profile is excited by the horizontal kick of the PQM. The RMS beam sizes in the PQM and PSM injections are plotted in Fig. 7 as a function of the turn number. For the sake of comparison, the estimated beam sizes were converted to the change ratio from the average beam size before the first turn. In the PQM injection, the horizontal beam size increases to twice the size before the kick, while in the PSM injection, the size remains almost constant. These results show that the PSM injection can realize an ideal top-up injection in which both the stored beam position and profile do not fluctuate at every injection.

The PSM injection has been introduced for user operation instead of kicker injection since January 2011. In the near future, we plan to conduct machine studies to minimize the residual stored beam oscillation and to improve the injection efficiency.

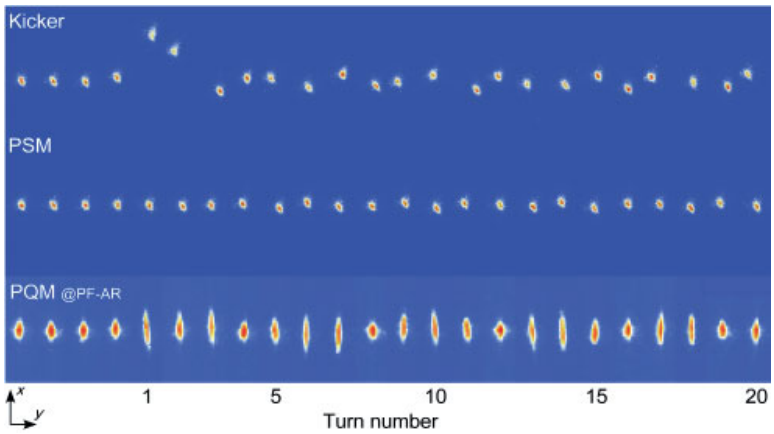

Figure 5
Turn-by-turn stored beam profiles in the kicker, PSM, and PQM injections measured by using a fast-gated camera. The data on the PQM injection were acquired at the PF-AR. Each injection magnet was fired at the first turn (turn number = 1).

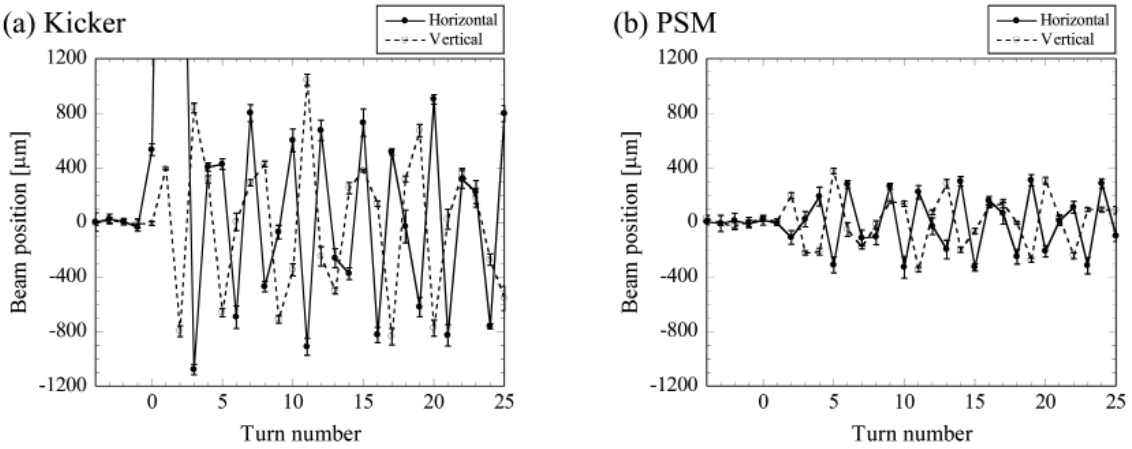

Figure 6
Beam positions of the stored beam in the kicker injection (a) and PSM injection (b). The horizontal displacement observed at the first turn of (a) is 5.5 mm.

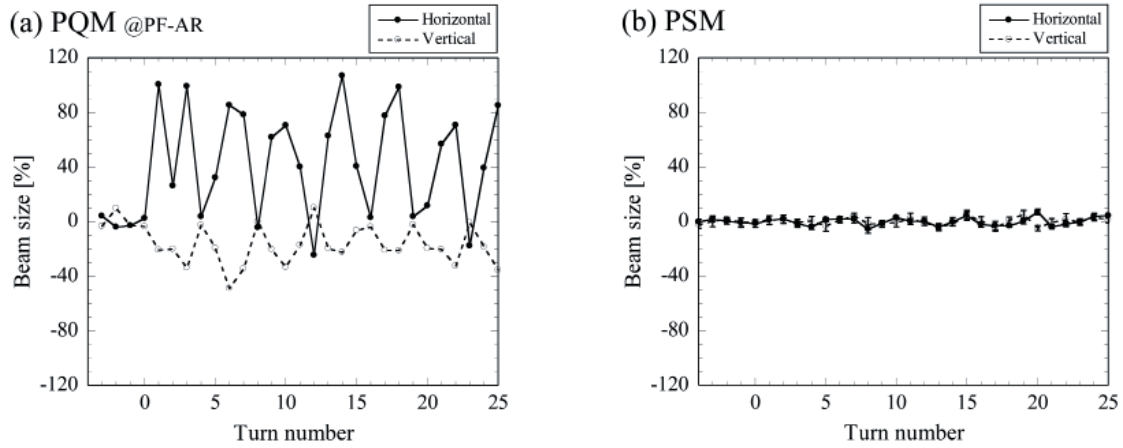

Figure 7
Beam sizes of the stored beam in the PQM injection (a) and PSM injection (b).

REFERENCES

[1] H. Takaki, N. Nakamura, Y. Kobayashi, K. Harada, T. Miyajima, A. Ueda, S. Nagahashi, M. Shimada, T. Obina and T. Honda, *Phys. Rev. ST-Accel. Beams* **13** (2010) 020705.
[2] K. Harada, Y. Kobayashi, T. Miyajima and S. Nagahashi, *Phys. Rev. ST-Accel. Beams* **10** (2007) 123501.
[3] A. Ueda, K. Harada, Y. Kobayashi and T. Mitsuhashi, *Proc. EPAC '04* (2004) 710.
[4] K. Tsuchiya and T. Aoto, *Proc. IPAC '10* (2010) 3153.

2-3 Update of the Power Supply Control System for Pulsed Injection Magnets at the PF Ring

During the summer shutdown in 2010, we updated the control system for the pulsed injection magnets at the PF ring. We succeeded in improving the reliability and flexibility of the system by replacing the old CAMAC based system with a programmable logic controller (PLC) based system. We also introduced an EPICS [5] based system which is used for most of the control systems at the PF ring.

At the PF ring, the stability of the stored beam has become important since user operation with top-up injection started in October 2009. However, the reliability and the flexibility of the injection control system were poor because it was old. The system consisted of a customized controller (KS controller) made by a power supply manufacturer, CAMAC crates with digital and analog interface boards, a personal computer with a crate controller I/F board, a workstation made by Hewlett-Packard (HP-UX) and graphical user interfaces (GUIs) written by Virtual Avionics Prototyping System (VAPS) [6]. Above all, there was no spare KS controller, the flexibility was low, and as a result, failure of the KS controller was fatal for the operation at the PF ring. On the other hand, most control systems at the PF ring are based on EPICS, so we decided to upgrade the injection control system to an EPICS based one (Fig. 8). We decided to replace the KS controller and CAMAC with a PLC and a touch panel made by KEYENCE and an oscilloscope made by Agilent, and to employ a fiber thermometer for measuring the bodies of kicker magnets. We also developed the GUIs using Motif Editor and Display Manager (MEDM) and Extensible Display Manager (EDM) of EPICS tools (Fig. 9).

REFERENCES

[5] http://www.aps.anl.gov/epics/.
[6] *PF Activity Report 1997* **15** (1997) 141.

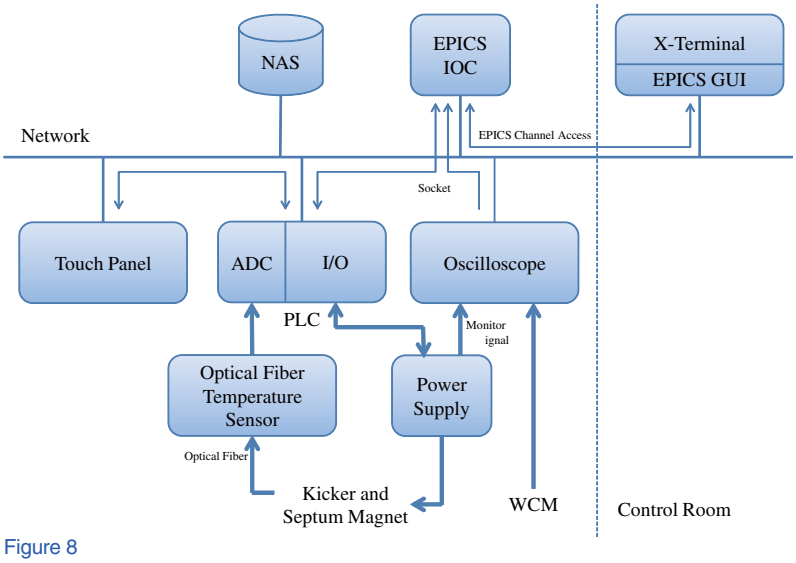

Figure 8
Conceptual diagram of the new control system.

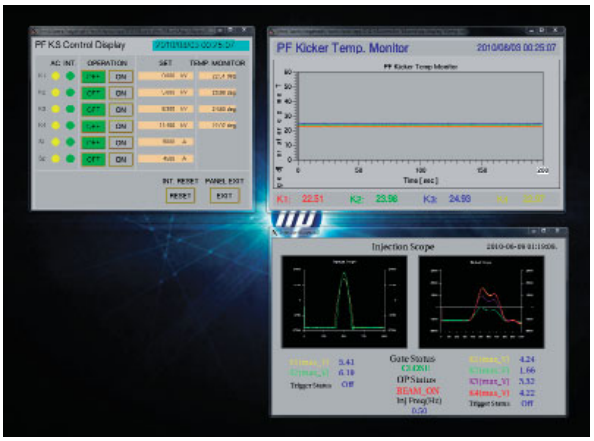

Figure 9
Example GUI screenshot for the new control system.

2-4 Status of the Fast Local Bump System for ID16

At the long straight section of 8.9-m length between B15 and B16 at the PF ring, two APPLE-II type undulators were installed with five identical fast bump magnets [Fig. 10 (a)]. The fast local bump achieves fast helicity switching, and is a good method for measuring the photon helicity-dependence of materials like circular and linear dichroism using a lock-in technique. The designed bump frequency is 10 Hz and the required bump angle is 0.3 mrad to separate photons from two undulators. The length of the bump magnets is 15 cm, and the capacity of the power supplies is ±50 V and ±100 A. The required maximum kick angle is about 2.4 mrad for the bump magnets K2 and K4. The magnetic current waveforms are sinusoidal with DC offset. For K2, for example, the current varies between 0 A to about 60 A sinusoidally. The bump system and current waveforms are shown in Fig. 10 (b). The system must be adjusted in order to fix the beam trajectories in two insertion devices and suppress the unwanted beam oscillation outside of the bump.

In order to correct the beam trajectories in the two insertion devices, fast beam position monitors (FPMs) shown in Fig. 10 (a) are used. When switching is off, the beam positions are measured by the slow averaged mode as shown in Fig. 11 (a). The angle of the photon beam axes of ID16-1 and ID16-2 can be fixed within 1 μm at the user beamline. During switching, the difference of the photon beam positions at the user beamline can be corrected within a few μrad to match the user's requirements by using the fast measurement mode of FPMs as shown in Fig. 11 (b).

For the designed goal, the amplitude of the unwanted beam oscillations around the ring should be suppressed to one tenth of the beam sizes, which are about 30 μm for the horizontal direction and 3 μm for the vertical direction. The kick angle of the bump magnets can be written as

$$\theta = K_{DC} + (K_{AC} + \Delta K)\sin(\omega t + \varphi_0 + \Delta\varphi)$$

where K_{DC} is DC bump, K_{AC} AC amplitude, ω angular frequency, t time, φ_0 initial phase, ΔK AC amplitude error, and $\Delta\varphi$ phase error. Taking AC components and linear error terms,

$$\Delta\theta_{AC} = \Delta K \sin(\omega t + \varphi_0) + K_{AC}\Delta\varphi\cos(\omega t + \varphi_0).$$

The amplitude errors of the bump magnets generate beam oscillations with the same phase as the bump, and the phase errors generate the oscillations with quadrature phase as shown in this equation. The measured unwanted beam oscillations are divided into the same phase component as the bump and the quadrature phase component. The amplitude errors and phase errors are corrected separately. After the amplitude and phase adjustments for K1–K5, the horizontal oscillations are suppressed to a few μm as shown in Fig. 12 (a). The skew quadrupole field of the undulator produces the orbit distortion in the vertical direction which cannot be suppressed by tuning the kicker magnets. In order to suppress these vertical oscillations, eight fast corrector

magnets (4 for the horizontal direction, 4 for the vertical direction) are installed [labelled “PHV” in Fig. 10 (a)]. A commercial all-in-one digital signal processing box (“iBIS”, from MTT Corporation), is adopted as a feed-forward controller. It has sixteen 16-bit ADCs and eight 16-bit DACs, with a real-time controller SH-4A. Software for the real-time part is developed using KPIT GNUSH tools which are freely available from a website, hence rapid application development and prototyping are easily achieved with the system. The signal processing clock is selected to be 20 kHz for now, which is fast enough to suppress the 10-Hz orbit movement. After feed-forward correction, vertical oscillations are also suppressed to a few μm as shown in Fig. 12 (b).

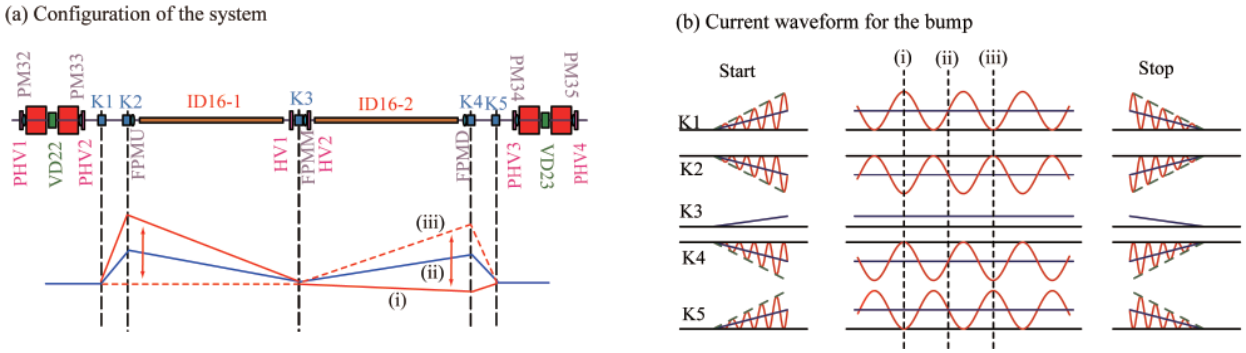

Figure 10
Configuration of the system, bump orbits and current waveforms. K1–K5 are the bump magnets, FPMs fast beam position monitors for adjustment of the fast bump, PMs normal beam position monitors for COD correction, VDs slow vertical steering magnets for the COD correction, HVs slow horizontal and vertical steering magnets to adjust the beam trajectory in two insertion devices, and PHV fast horizontal and vertical steering magnets for the feed-forward correction. In order to make the required fast bump, the DC bumps of the half heights are combined with the AC bump of the double peak-to-peak amplitude. In order to illustrate the DC and AC bumps, the beam trajectories in the two insertion devices are slightly shifted in the figure. In practice, DC orbit corrections are needed to fix the photon axis of the two insertion devices for the user beamline. At the timing (i), the bump angle is maximum in ID16-1 and only photons from ID16-2 are delivered to the user beamline, and vice versa at timing (iii). At (ii), AC amplitude is zero and there is only the DC bump, and about half of the photons from both ID16-1 and ID16-2 are delivered.

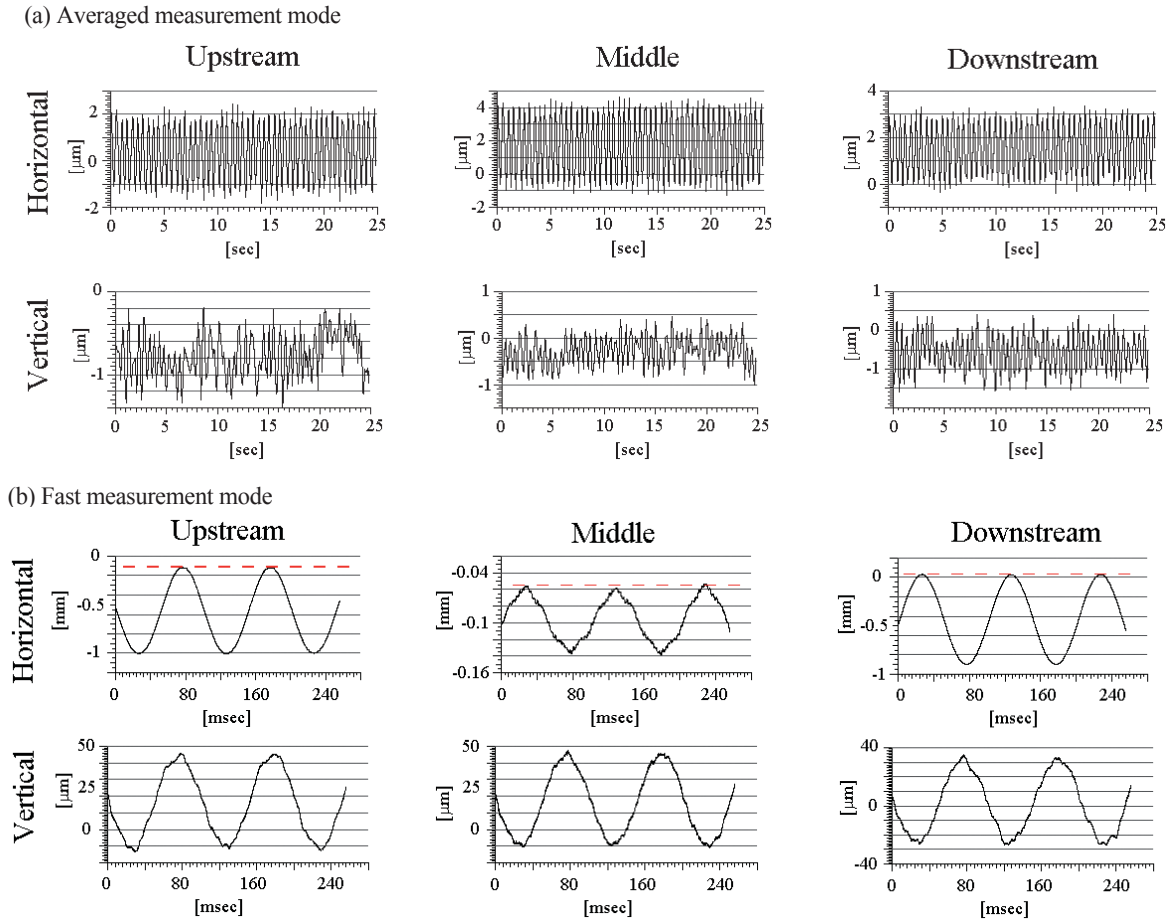

Figure 11
Example of beam position measurement by FPMs at the bump. For the averaged mode (a), beam positions can be measured with 1 μm accuracy. For the fast measurement with 10-Hz switching (b), the beam positions of the instance at the bump off (shown by red dotted line) are corrected by adjustment of the DC bump.

(a) Beam oscillation after adjustment of kicker magnets

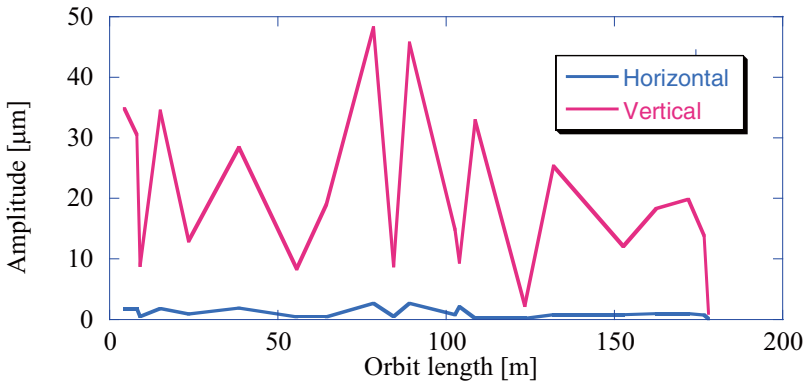

(b) Beam oscillation with vertical feed-forward correction

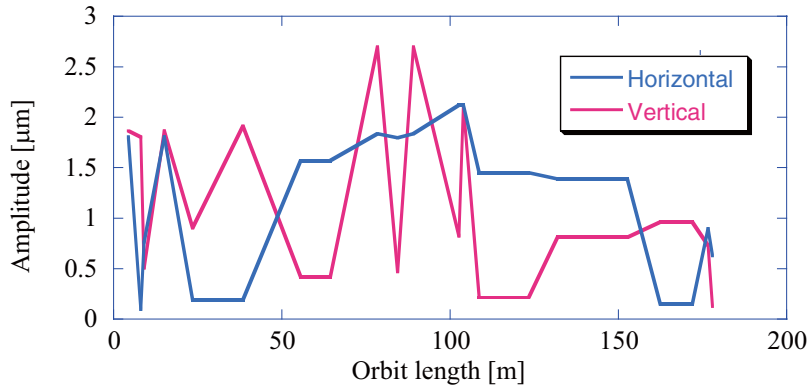

Figure 12
Beam oscillation around the ring with 10-Hz switching.

2-5 Construction and Operation of the U#16-2

We have been developing a rapid-polarization-switching source at the B15-16 straight section in the PF 2.5-GeV ring. The source consists of two tandem APPLE-II-type elliptically polarizing undulators (EPU), namely U#16-1 and U#16-2, and a fast kicker system. These two EPUs are designed to obtain soft X-rays in the energy region from 200 eV to 1 keV under various polarization states. As the first step, we constructed U#16-1 and installed it in the PF ring in March 2008. Operation of U#16-1 for user experiments has been ongoing since April 2008.

As the next step, a second EPU, U#16-2 was constructed in 2010. The magnetic adjustment of U#16-2 was finished in March 2010, and we then performed magnetic measurements of U#16-2 under the various conditions of all operation modes. The magnetic field measurement for U#16-2 took three months.

After the magnetic measurements, U#16-2 was installed in the PF ring in August 2010. Figure 13 shows a photograph of U#16-1 and U#16-2 at the B15-16 straight section after installation of U#16-2.

U#16-2 is identical to U#16-1, and has an APPLE-II-type magnetic arrangement. The period length of the EPU is 56 mm and the periodicity number is 44. U#16-2 has four variable rows of magnetic arrays to change the polarization states, and a gap-driving mechanism to change the photon energy. By moving the four rows of magnetic arrays individually, we can use U#16-2 as both the usual APPLE-II type EPU and as an adjustable phase undulator (APU). In APU, we move the top pair of magnetic rows longitudinally with respect to the bottom pair; however, the gap is fixed to change the photon energy.

We measured the magnetic distribution of U#16-2 in both the usual EPU mode and the APU mode. Examples of the magnetic measurements of the EPU mode for various polarization states are shown in Fig. 14. The electron orbits at several typical gaps are shown, which were calculated based on data measured in the circular polarized mode.

U#16-2 became operational for user experiments after commissioning in the PF ring. U#16-1 and U#16-2 are used under the APU symmetric mode. Experimental users can change the photon energy and the polarization state of both U#16-1 and U#16-2 at any time during operation of the PF ring. The typical available polarization modes are circular polarization (B_x/B_y = 1), elliptical polarization (B_x/B_y = 1/2), and linear polarization in the horizontal and vertical directions.

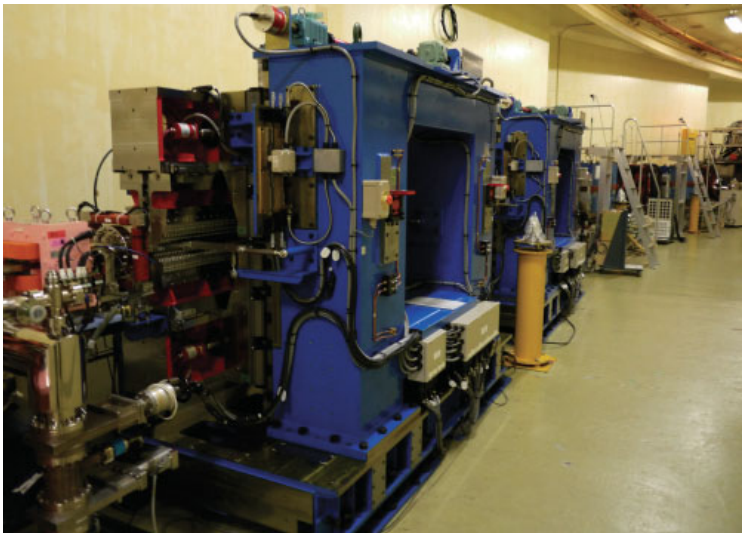

Figure 13
Photograph of U#16-1 and U#16-2 at the B15-16 straight section. U#16-2 is toward the front.

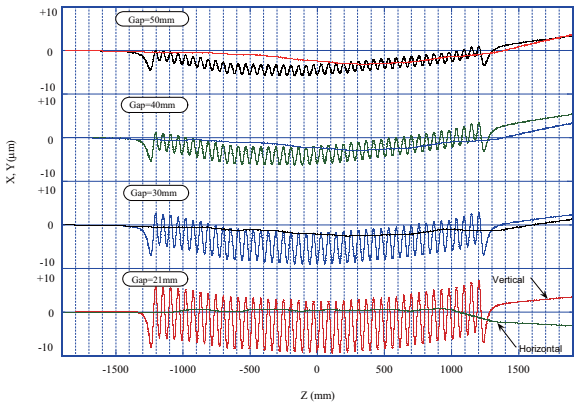

(1) The calculated orbit of the linear polarization mode in the horizontal direction

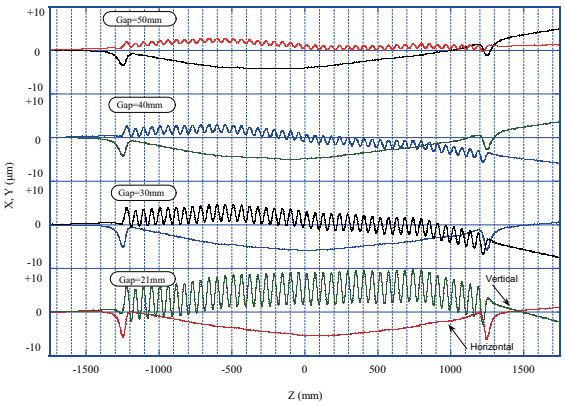

(2) The calculated orbit of the linear polarization mode in the vertical direction

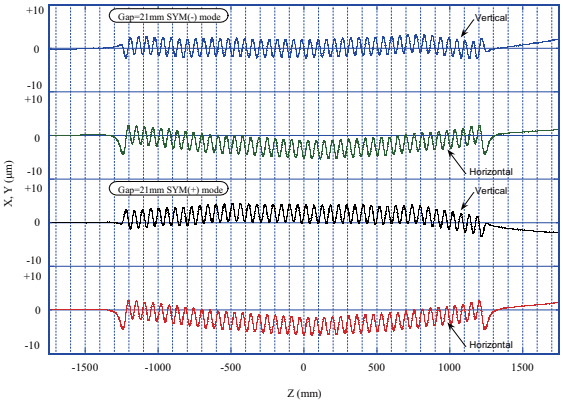

(3) The calculated orbit of the circular polarization mode

Figure 14
Results of magnetic measurements of U#16-2.